PROCEEDINGS OF SCIENCE

Thermal Shocks as a Detection Method for Heavy Exotic Particles in Neutrino Telescopes

C. Locatelli,[a] **A. Obertacke,**[a,*] **H. Toribuchi**[a] **and D. Zhang**[a]

[a] *International Center for Hadron Astro-Physics,Chiba University, Japan*

E-mail: aobertacke@icecube.wisc.edu

Many well-motivated extensions of the Standard Model predict the existence of extremely heavy particles, such as Q-balls and Nuclearites. However, detecting electrically neutral or non-relativistic particles remains an experimental challenge.
As these nearly macroscopic particles traverse matter they deposit energy through friction, heating the medium to plasma temperatures. The resulting black-body radiation can be detected using generic light sensors, yet the plasma light yield in media, such as water and ice, is subject to considerable theoretical uncertainties.
Rare particle searches benefit from large detector volumes. The world's largest instrumented detectors are neutrino telescopes that use water or ice as detection medium. To investigate the feasibility of this detection method at neutrino telescopes, we simulated plasma production in ice by exposing it to an intense laser beam.
We present measurements of the resulting light yield and time evolution discussing their implications for exotic particle searches in neutrino observatories.

39th International Cosmic Ray Conference (ICRC2025)
15–24 July 2025
Geneva, Switzerland

*Speaker

PoS(ICRC2025)516

1. Exotic physics searches with thermal shocks

Thermal shock refers to the phenomenon wherein a heavy particle traverses a medium, depositing a lot of energy along its path and inducing local heating by friction. In solid media such as ice, this localized heating can raise the temperature to several thousand Kelvin, leading to the formation of a high-pressure region. Plasma generation in the wake of a thermal shock arises when the deposited energy elevates the local temperature to levels sufficient for ionizing atoms and molecules. The characteristics of the resulting plasma, including its density, ionization degree, and radiative properties, are essential in determining its detectability with optical instruments. This process enables the detection of signatures from exotic particles such as *Q-balls* [1].

Q-balls are heavy exotic particles that have been proposed as potential candidates for Dark Matter. They are non-topological solitons arising from scalar field configurations, and are predicted in certain super-symmetric extensions of the Standard Model [1, 2].

The energy loss by friction of a heavy particle propagating through a medium is dominated by its geometric cross section [1]

$$\frac{dE}{dx} = -\rho\sigma v^2 \tag{1}$$

where ρ is the medium density, v is the velocity of the particle, and σ is its effective cross-sectional area. For Q-balls, the cross section is determined by their effective radius R, such that $\sigma = \pi R^2$. The radius R depends on the Q-ball's mass or baryon number Q, with the theoretical relation $R = R(M) \propto Q^{1/4}$ [2] and a potential lower limit at the Bohr radius a_0 of $\sigma = \pi a_0^2 \approx 10^{-16}\,\mathrm{cm}^2$ [3].

Thermal shock waves are expected to emit blackbody radiation, see Fig. 6. Particle searches based on such thermal radiation require an estimation of the emitted light. A rough theoretical estimation derives the energy to *photon conversion factor* to be $\eta = 3 \times 10^{-5}$ with [1]

$$\frac{\mathrm{d}N_\gamma}{\mathrm{d}x} = \eta \cdot \frac{\frac{\mathrm{d}E}{\mathrm{d}x}}{\langle E_\gamma \rangle} \tag{2}$$

the number of photons N_γ emitted per unit length $\mathrm{d}N_\gamma/\mathrm{d}x$, and the energy loss rate $\mathrm{d}E/\mathrm{d}x$. The value of the conversion factor η is subject to significant uncertainties due to the complexity of the shock's optical properties and temperature [4]. The average energy of emitted photons at a temperature T is given by the fraction of total emitted energy and number of emitted photons [5]

$$\langle E_\gamma \rangle = \frac{\int B_\nu \,\mathrm{d}\nu}{\int \frac{B_\nu}{h\nu}\,\mathrm{d}\nu} = \frac{\int_0^\infty E \cdot B(E,T)\,\mathrm{d}E}{\int_0^\infty B(E,T)\,\mathrm{d}E} = \frac{\pi^4}{30\,\zeta(3)} k_B T \approx 2.70\, k_B T \tag{3}$$

Here, $B(E,T)$ is the Planck distribution, and k_B is the Boltzmann's constant. Assuming the theoretical expectation of the energy conversion factor η given best guesses of the plasma temperature ($10^5 \sim 10^7$[4]) results in a rather high number of photons emitted around a Q-ball track (Fig. 1) that is expected to be detectable.

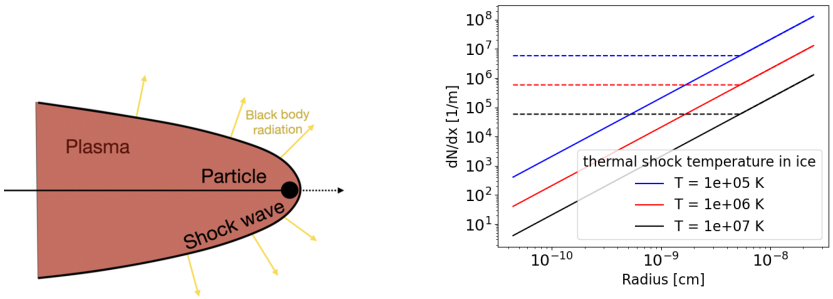

Figure 1: Left: Illustration of plasma buildup in a medium along the track of an incident particle, called thermal shock. **Right:** The number of photons emitted per unit length $\mathrm{d}N_\gamma/\mathrm{d}x$ depends on the effective radius of a Q-ball. The temperature T corresponds to the plasma temperature generated by thermal shock in ice. The dashed lines represent lower bounds on the light yield, corresponding to the case where the effective radius is equal to the Bohr radius.

To search for rare exotic particles, such as Q-balls, extreme large detectors (with correspondingly high sensitivity) are required. Neutrino telescopes, that are designed for Cherenkov light detection, provide the largest possible detection volumes and optical sensitivity to observe the thermal shock of heavy particles. The detection media are natural water and ice. In order to start with a simpler experimental setup, this work starts with the investigation of the solid medium that is used by the *IceCube Neutrino Observatory*.

The IceCube detector is a cubic-kilometer-scale high-energy neutrino telescope embedded within the Antarctic ice at the South Pole [6]. The IceCube in-ice array comprises of 5160 Digital Optical Modules (DOMs) distributed over one cubic kilometer in Antarctic ice and sensitive to visible light in the range of 300 nm – 650 nm [6]. The temperature of the Antarctic ice depends on the depth and ranges from −43 °C to −20 °C [7].

Neither for the conditions at IceCube nor similar conditions, there are any measurements of the optical emissions induced by thermal shock. Therefore, the goal of this work is to measure the conversion factor η in a laboratory experiment.

2. Experimental setup

In this experiment, the particle path is emulated by a strong infrared laser shooting into ice, see Fig. 2 (right). A 1 kHz laser pulse is generated as a pumping laser and focused onto a laser medium of yttrium vanadate doped with neodymium ions. After inversion, the medium emits a laser beam with a wavelength of 1342 nm, a diameter of 1 mm, and a power of up to 1 W, along with the low-energy pumping laser at 840 nm. The pumping laser light is reduced by a factor $5.6 \cdot 10^{-9}$ by two long-pass[1] and one dichroic[2] filters, along with two 5 mm diameter apertures. The laser beam then enters an ice sample composed of ultra-purified water in order to ensure consistent and repeatable quality, see Fig. 2 (left). A 1-inch-diameter *photomultiplier tube* (PMT) arranged in single-photon counting mode[3] is positioned above the ice sample to detect light from the ice sample.

[1] Thorlabs FELH1050
[2] Thorlabs DMLP1180
[3] Hamamatsu R1924 with quantum efficiency of about 26% and a darkrate at 20°C of about 60 Hz.

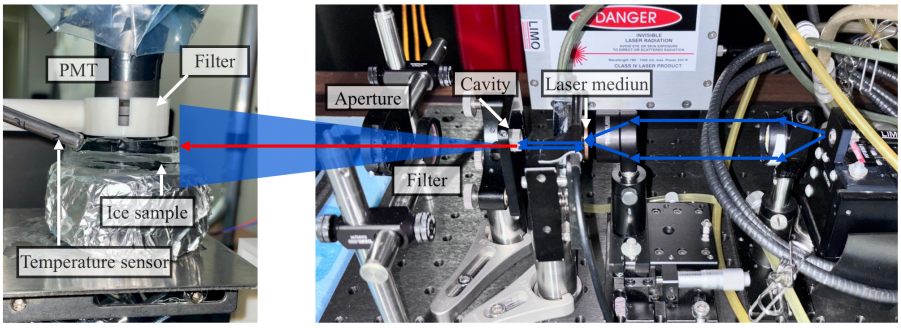

Figure 2: Experimental setup to produce thermal shock in ice with a strong infrared laser. The customized laser setup is shown on the right. The blue arrows indicate the parallelization and concentration of the pumping laser on the laser medium. The laser path (red arrow) along the pumping laser light (blue cone) is shown to impact an ice sample in the left figure. On the left side is the setup for the light detection. A white arm is used to place two shortpass edge filters[4] between the ice sample and the PMT to remove scattered light. A temperature sensor is shown on the left side of the ice.

To ensure the laser operates under stable room-temperature conditions while maintaining the observation volume at −40°C in total darkness, a wooden enclosure was constructed. This enclosure is divided into three sections: a room-temperature zone, a cryogenic zone, and a dry ice storage zone. The cryogenic zone is thermally connected to the dry ice zone by a thin aluminum plate, with dry ice serving as the cooling source. Additionally, the interior of the cryogenic zone is lined with 6 cm-thick styrofoam panels to provide thermal insulation. A hole connects the cryogenic zone and the laser zone to allow the laser beam to pass through. Two of the pumping laser filters are embedded within this hole. During the experiment, the photon pulses were recorded alongside environmental parameters like ambient light, temperatures of the zones and ice temperature in order to identify possible correlations.

One limitation of this experiment is that we were unable to measure the laser power while the PMT was operating. However, we found that the laser power is quadratically correlated with the temperature of water that is used to cool the laser medium using a chiller. To determine the laser power while the PMT is operating, we conducted calibration measurement both before and after the experiment.

3. Experimental observations

3.1 Background estimation

Early measurements show an average amount of detected photons per laser pulse of 0.05 to 1.44 which depends on the temperature of the ice sample or the temperature change in the ice sample as well as the optical geometry of the setup, see Fig. 3. Background from thermal noise of the photomultiplier was found to be negligible[5] beyond the first hour of measurements. A dependency of the pulse number to the laser power, that oscillate with $\sim 40 - 50$ min, cannot be resolved.

[4] Thorlabs FESH0800 with a transmission from 500 nm to 789 nm and a transmission on the scale of 10^{-9} for both, the pumping laser and main laser

[5] see as an example the baseline in Fig. 5

Significant fluctuations of the pulse count, such as visible in Fig. 3 (left) after 42 h, were regularly observed during drastic temperature changes in the experiment (see also Fig. 4).

In order to quantify background from scattered laser light into the photomultiplier, short-pass filters were added to the setup as described before and removed during the running measurement after 7 h, see Fig. 3 (right). No measurable change in the photon number was observed. In conclusion background effects are sub-dominant in the developed setup.

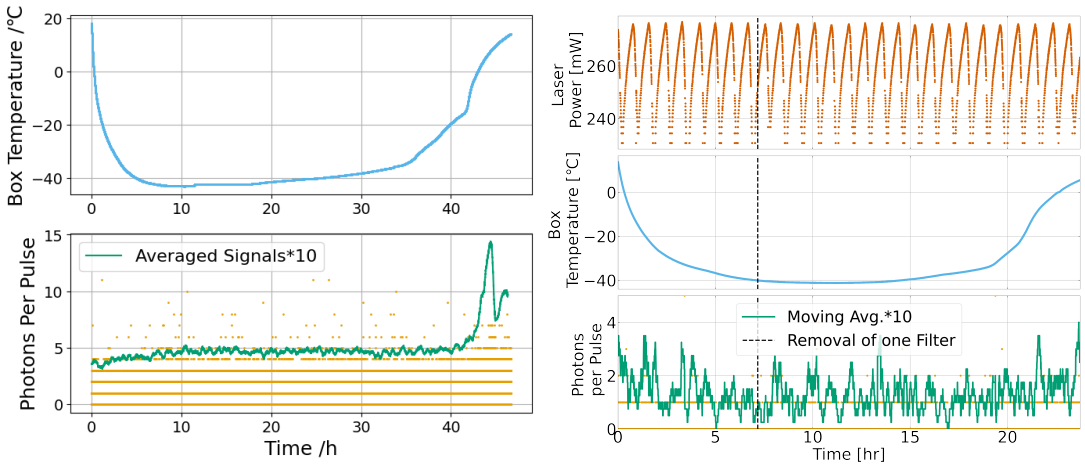

Figure 3: Development of recorded measurement values over the full term of 2 measurements. **Left:** The temperature in the experimental compartment is shown in the top half, which is supposed to be in thermal equilibrium with the temperature of the ice sample at minimal temperatures. The bottom half shows recorded PMT pulses per laser shot. On the raw PMT waveforms during one laser shot (plus extra time of ±10%), a pulse finder algorithm is applied with a trigger of 2 mV in order to get the amplitudes and times of all photons. The running average is amplified to ease reading. At the lowest temperature of −43.19°C an average of 0.502 photons per laser pulse were recorded. **Right:** The laser power oscillation (estimated from the chiller temperature) is shown as top panel for this measurement. At 7 h (dashed line) a short-pass filter is removed between the ice and photomultiplier. The average of photons per laser pulse at stable, i.e. lowest temperatures, is derived to be 0.141.

3.2 Signal characterization

The learning from early measurements lead to an improvement in the setup as well as the read-out system that increased the statistics of evaluated laser shots by more than 2 orders of magnitude. With the resulting finer distributions, the signal can be characterized as follows.

In all measurements, a channel of 3 cm length and 3 mm width can be observed in the ice after the measurement.

As observed before, the photon count shows variability at extreme temperature changes of the ice and a correlation at slow temperature changes, see Fig. 4 (left). Additionally, a strong linear correlation with the chiller temperature can be observed, see Fig. 4 (right). As the chiller temperature is used to monitor the laser power, the number of photons is correlated with the oscillating laser intensity.

The temporal distribution of photons is compared to the laser and pumping-laser amplitudes in Fig. 5 (right). The amount of detected photons begins to increase after the start of the pumping

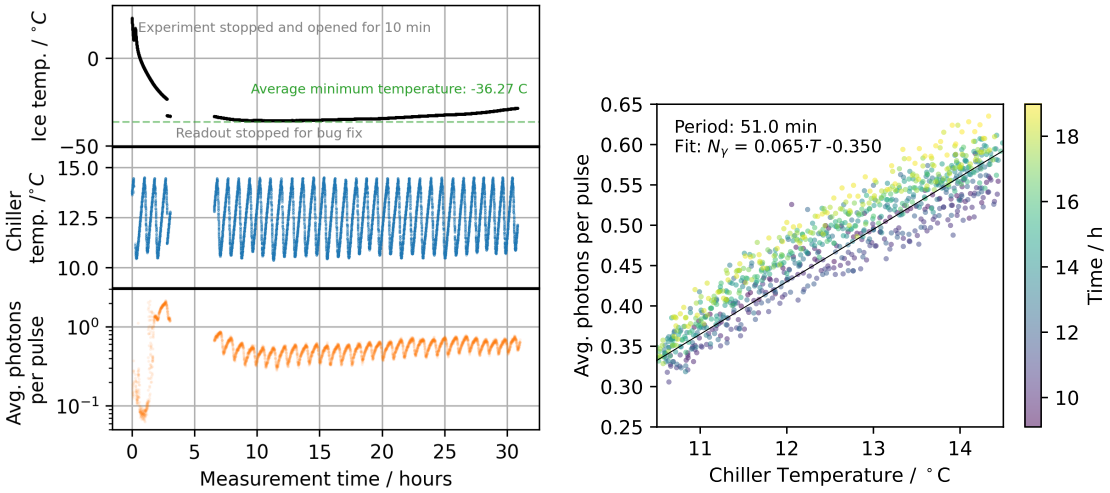

Figure 4: Left: Development of recorded measurement values for an experiment with increased statistics in comparison to Fig. 3. The chiller temperature is used to predict the laser power. **Right:** The correlation of chiller temperature and photon count is shown and fit using a linear function.

laser, stagnating at about 65 µs. Once the main laser switches on, the number of photons increases progressively.

The visibility of the pumping laser in the temporal distribution suggests that photons from the pumping laser arrives both directly and via scattering in the ice at the PMT. Despite its spectral sensitivity to visible light, the PMT does have limited sensitivity at 840 nm. A control measurement without ice confirms that a high number of photons impact the PMT directly, despite apertures and filters. Despite of that, the light by the pumping laser does not impact the measurement results nor the interpretation. We found no indication that the IR laser photons can be and was detected by the PMT neither directly nor after scattering in the ice.

The shape of the build-up of photons in the temporal distribution, while the strong IR laser is shooting, is dissimilar to the laser waveform as well as its energy deposition. Even after both lasers are switched off at 145 µs, photon detections persist for up to additional 10 µs and an exponential decay can be observed.

4. Analysis

A ray tracing program was written to obtain the number of emitted photons near the laser track from the observed averaged photon count per laser shot, see Fig. 6 (left). The ice is modeled using Henyey-Greenstein scattering [8] with an asymmetry parameter of 0.9. Dimensions of the ice sample and its distance to the PMT are adjusted for all measurements separately. Reflection at the aluminum foil below the ice is considered, but negligible. As soon as a ray leaves the ice, it is discarded if it does not hit the PMT. The laser beam is modeled as an isotropically emitting line source along with absorption according to the Lambert-Beer's law, using the absorption coefficient from Ref. [9]. The emission of photons from this line is assumed to be linearly dependent on the absorption. Thus, most of the light is emitted near the entrance of the laser beam into the ice.

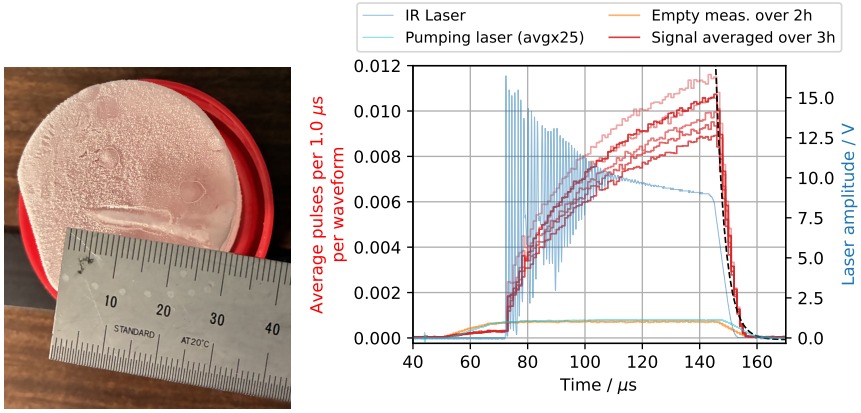

Figure 5: Left: Photograph of an ice sample after measurement showing the channel melt by the laser into the ice. **Right:** Time-resolved distribution of the photons per laser pulse in a measurement with ice (red) and without ice (orange) in comparison to averaged waveform of the pumping laser (amplified by factor 25, cyan) and a characteristic waveform of the IR laser (blue). The trigger from the laser generator is visible at $\sim 45\,\mu$s. The pumping laser is switched on for $100\,\mu$s. The IR laser is emitted $\sim 20\,\mu$s later and oscillate before settling to a stable amplitude. The black dashed line shows the decay time after the laser is switched of with a decay constant of 3.3 µs (IR laser shape subtracted).

For the evaluated measurements, 5.7% to 16.3% of the photons emitted from the laser channel arrive at the PMT and produce a visible hit, taking the measured radial PMT quantum efficiency into account as well as the trigger threshold for photon pulses. From this, a number of 2.3 to 24 photons emitted from the laser channel per shot can be derived that appear to be correlated with the averaged laser power, see Fig. 6 (middle). The corresponding thermal shock conversion factor is on the level of $\eta_{\text{measured}} \approx 10^{-13}$, considerably lower than estimated by theory, see Eq. 2.

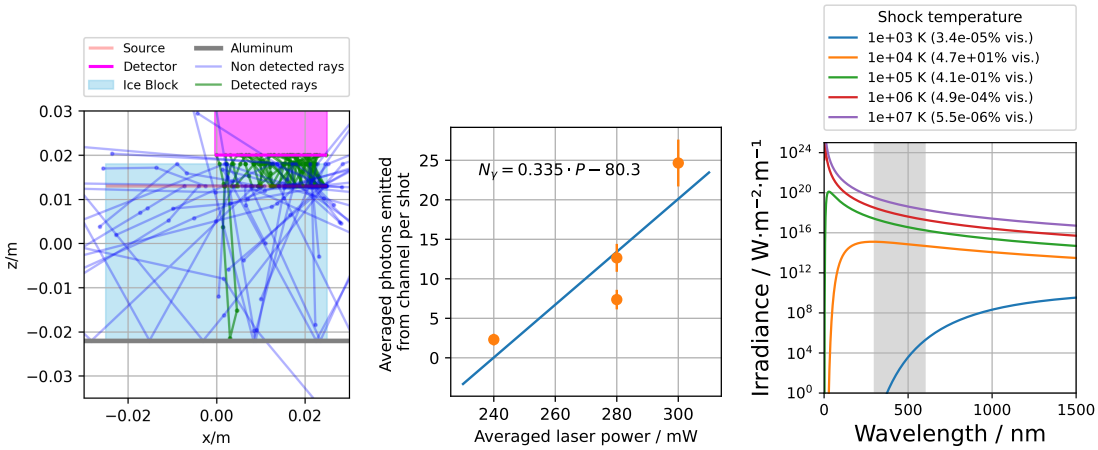

Figure 6: Left: Two dimensional illustration of a sub-sample of simulated rays emitted from the laser channel. The number of detected rays vs non-detected rays is arbitrarily increased. **Middle:** Correlation of the emitted photons per laser shot from the laser channel to the averaged laser power of the corresponding measurement. **Right:** Black body radiation spectrum depending on different temperatures of the medium and the fraction that can be detected by the given PMT.

5. Discussion and outlook

Based on above observations and analysis, we derived a model of the observed process with the following calculation: the laser beam cuts a channel into the ice in subsequent shots by depositing up to 10^9 J/m^3 of energy up to approximately 3 cm in the ice. The first shot suffices to heat and melt the ice, as well as heat the water in the channel up to ~ 400°C at a pressure of ~ 95 MPa. With the third shot the temperature is increased to ~ 550°C at a pressure of ~ 430 MPa. Cooling from the ice as well as pressure release from the water is too slow between the laser pulses and therefore negligible.

After the 3rd shot the water is beyond the critical point and a fast shock wave can develop at $\sim$ Mach 47 in the ice. This shock induces a temperature of up to 4700 K near the channel walls that cools rapidly by expansion, e.g. within 2 µs below 1000 K. Due to the long laser beam pulse of 80 µs, the channel temperature slowly increases to ~ 800 K while the shock temperature near the channel increases to ~ 8000 K, taking expansion cooling during this time into account.

In conclusion, the given laser has insufficient power to heat the full volume of the laser channel to plasma temperatures as opposed to our intention.

Instead, the deposited energy suffices to produce critical water that produces a mechanical shock wave in the ice that in turn leads to a thin shell of plasma temperature that quickly expands, i.e. cools. The Black-Body radiation from low-temperature plasma emits $\epsilon_{\mathrm{BB}} \approx 3 \cdot 10^{-5}\%$ to 5% of its total spectrum within the PMT's spectral sensitivity range. In that case, the energy conversion factor $\eta_{\mathrm{model}} = \eta_{\mathrm{measured}}/\epsilon_{\mathrm{BB}} \cdot 100$ increases to up to 10^{-7} depending on actual temperature in the channel.

The experiment will accordingly be adjusted to use a stronger laser with shorter pulse duration from hereon. A measurement of the emitted spectrum will help to determine the channel's temperature. Additionally, the acoustic and radio emissions of the thermal shock are planned to be recorded. Only for the latter, there are extensive studies to which our measurements can be compared.

Acknowledgements: The authors are grateful to Takashige Omatsu and A. Srinivasa Rao from the Molecular Chirality Research Center at Chiba University for constructing and providing a customized laser.

References

[1] A. D. Rújula and S. L. Glashow, *Nature* **312** (1984) 734 – 737.
[2] A. Kusenko *et al.*, *Physical Review D* **72** (2005) 025015.
[3] D. Bakari *et al.*, *Astroparticle Physics* **15** (2001) 137 – 147.
[4] A. Pohl, *Search for Subrelativistic Particles with the AMANDA Neutrino Telescope*. PhD thesis, Uppsala University, 2009. Doctoral Dissertation.
[5] J. M. Marr and F. P. Wilkin, *American Journal of Physics* **80** (2012) 399 – 405.
[6] **IceCube** Collaboration, M. G. Aartsen *et al.*, *JINST* **12** (2017) P03012.
[7] **IceCube** Collaboration, *The IceCube Neutrino Observatory VI: Ice Properties, Reconstruction and Future Developments*. 2013. In proceedings of ICRC 2013, arxiv:1309.7010.
[8] **IceCube** Collaboration, M. Ackermann *et al.*, *Journal of Geophysical Research* **111** no. D13, (2006) .
[9] S. Warren and R. Brandt, *Journal of Geophysical Research* **113** no. D14220, (2008) .